第 33 卷第 3 期
2017 年 3 月

无 机 化 学 学 报
CHINESE JOURNAL OF INORGANIC CHEMISTRY

Vol.33 No.3
493-500

铌酸锰–还原氧化石墨烯复合光催化剂的构建以及可见光下降解亚甲基蓝

顾 巍[1] 严 铭[2] 孙 林[1] 施伟东*,[1]

([1]江苏大学化学化工学院,镇江 212013)

([2]江苏大学材料科学与工程学院,镇江 212013)

摘要:通过水热法和光还原方法成功地制备了铌酸锰–还原氧化石墨烯复合光催化剂。这种复合光催化剂可以明显地提高光催化降解亚甲基蓝的光催化活性,降解效率在 60 min 内达到了 78.2% ,是单体铌酸锰降解效率的 2 倍。通过活性物质捕获实验的研究,增强的光催化性能可以归因于还原氧化石墨烯加速了光生电子–空穴的分离效率,进而解决了低光催化活性的问题。

关键词:铌酸锰–还原氧化石墨烯;光催化剂;亚甲基蓝;可见光

中图分类号:TQ032.42 **文献标识码**:A **文章编号**:1001-4861(2017)03-0493-08

DOI:10.11862/CJIC.2017.054

Fabrication of RGO-$MnNb_2O_6$ Photocatalyst with Enhanced Visible Light Efficiency in Photocatalytic Degradation of Methylene Blue

GU Wei[1] YAN Ming[2] SUN Lin[1] SHI Wei-Dong*,[1]

([1]*School of Chemistry and Chemical Engineering, Jiangsu University, Zhenjiang, Jiangsu* 212013, *China*)

([2]*School of Material Science and Engineering, Jiangsu University, Zhenjiang, Jiangsu* 212013, *China*)

Abstract: RGO-$MnNb_2O_6$ photocatalysts were successfully prepared through the hydrothermal and photo-reduction processes. Compared with single $MnNb_2O_6$, the RGO-$MnNb_2O_6$ composites could significantly enhance photocatalytic activity for the degradation of methylene blue under visible light irradiation. Within 60 min, 78.2% of the methylene blue was removed by the optimum sample (3% RGO-$MnNb_2O_6$), which was about 2 times higher than that of the individual $MnNb_2O_6$. By further study based on the active species trapping experiments, the enhanced photocatalytic property could be ascribed to the crucial role of RGO, which widely accelerated the separation of photogenerated electron-hole pairs. In general, the RGO hybridized with $MnNb_2O_6$ could address the problem of low photocatalytic activity.

Keywords: RGO-$MnNb_2O_6$; photocatalyst; methylene blue; visible light

0 Introduction

Swage release from industries generated a fearful puzzle for environmental pollution. The discharge of waste water was often detected including organic dyes, which were usually hazardous to the human health[1-5]. Therefore, the elimination of organic pollutes from aqueous environments has become a forcible environmental problem. However, the traditional treatments were often constrained by the low efficiency and high cost[6-7]. Recently, the photocatalytic oxidation has been established to be a promising technique for

收稿日期:2016-09-13。收修改稿日期:2016-12-30。

国家自然科学基金(No.21303074)、中国博士后科学基金(No.2015T80500)和江苏省自然科学基金(No.BK20141304)资助项目。

*通信联系人。E-mail:swd1978@ujs.edu.cn

environmental remediation and provided an efficiency tool for the degradation of organic dyes[8-13]. Up to now, a lot of researchers were focused on the conventional UV-driven titanium dioxide (TiO_2) for the dyes degradation. However, the wide band gap (3.2 eV for anatase) conspicuously confined its photocatalytic applications under visible light illumination[14-15]. Hereby, it is necessary to develop the high efficiency visible-light-driven photocatalysts[16-22].

On the one hand, niobate semiconductors have been widely investigated in photocatalysis due to their chemical and electrochemical stability. $MnNb_2O_6$, as a novel transition metal niobate photocatalyst, has attracted much attention in photocatalytic applications due to its narrow band energy of 2.2 eV. Hu et al. reported that the 3D flower-like nanostructures $MnNb_2O_6$ exhibited the photocatalytic performance for photodegradation of methylene blue (MB) under visible light irradiation[23]. However, surface properties of $MnNb_2O_6$ such as fast charge recombination at surfaces and weak surface adsorption ability have greatly limited the further improvement of its photocatalytic activity.

On the other hand, reduced graphene oxide (RGO) has been proved to be an excellent media for electron transfer because of its excellent electrical conductivity, high specific surface areas and excellent electronic mobility. A large number of RGO based photocatalysts have been successfully constructed for enhancing photocatalytic performances[26-27]. For example, Amal and colleagues prepared $BiVO_4$-RGO composite using a facile single-step photocatalytic reaction. Remarkable 10-fold enhancement in photoelectron chemical water splitting reaction was observed on $BiVO_4$-RGO composite compared with pure $BiVO_4$ under visible illuminations[28]. Shi and his group had investigated the $BiPO_4$-RGO samples and showed that after introducing the RGO, the photocatalytic activity have been improved by enhancing the separation of charge carrier[29]. Hence, we envision that the RGO can be regarded as an ideal electron mediate and supporter for $MnNb_2O_6$ photocatalyst, which will simultaneously facilitate the charge migration and prolong the charge lifetimes by suppressing the recombination of photogenerated electrons and holes.

Herein, we prepared the simple yet efficient visible-light-driven RGO-$MnNb_2O_6$ photocatalysts by the simple hydrothermal and photo-reduction methods. MB was chosen as target pollutants to explore the photocatalytic performance. Furthermore, tentative mechanism of the enhanced photocatalytic activities was also discussed based on the active species trapping experiments.

1 Experimental

1.1 Syntheses of GO and $MnNb_2O_6$

GO was synthesized via the oxidation of graphite using the improved Hummers′ method[30]. The synthesis process of $MnNb_2O_6$ was as follows: firstly, 0.5 g Nb_2O_5 and 3.37 g KOH were added into 60 mL of distilled water and then transferred into a 100 mL Teflon-lined stainless steel autoclave at 180 ℃ for 3 days. After cooling naturally, the clear solution of $[Nb_6O_{19}]^{8-}$ was obtained. Then, the above solution (4 mL) was diluted with 10 mL distilled water. The pH of obtained aqueous solution was adjusted to 7.8 by the addition of HCL solution. After that, 0.035 g $MnCl_2\cdot 4H_2O$ and 1 g K_2SO_4 were dissolved in above solution with continuous stirring for 30 min. Finally, the obtained precursor was transferred into a 50 mL Teflon-lined stainless autoclave at 260 ℃ for 24 h. The products were filtered, washed with distilled water, and dried in a vacuum at 60 ℃ for 12 h.

1.2 Synthesis of RGO-$MnNb_2O_6$

RGO-$MnNb_2O_6$ samples were synthesized through the method of surface assembling. Typically, a certain amount of GO (1, 3 and 5 mg) was dissolved in 100 mL water to form a transparent solution. Then 100 mg $MnNb_2O_6$ in certain ratio were added into the above GO solution under vigorous stirring for 30 min. The obtained suspension was exposed to the full-range irradiation of a 300 W xenon lamp for 3 h to reduce the GO into RGO. The final product collected by centrifugation, dried at 60 ℃ in air, which referred to as 1% RGO-$MnNb_2O_6$, 3% RGO-$MnNb_2O_6$, and 5% RGO-$MnNb_2O_6$.

1.3 Characterization

X-ray diffraction (XRD) patterns measurement was undertaken using a D/MAX-2500 diffract meter (Rigaku, Japan) with a nickel-filtered Cu $K\alpha$ radiation source (λ=0.154 056 nm, U=50 kV, I=300 mA, 2θ=5°~80°). The X-ray photoelectron spectros-copy (XPS) was obtained by a Thermo ESCALAB 250X (America) electron spectrometer using 150 W Al $K\alpha$ X-ray sources. The scanning electron microscopy (SEM) was obtained by the Hitachi S-4800 eld emission SEM (FESEM, Hitachi, Japan) to observe the morphology of the as-prepared samples. Transmission electron microscopy (TEM) and high-resolution trans-mission electron microscopy (HRTEM) were gathered on an F20 S-TWIN electron microscope (Tecnai G2, FEI Co.), equipping with a 200 kV accelerating voltage. The photoluminescence (PL) spectra for solid samples were obtained on a F4500 (Hitachi, Japan) photoluminescence detector. UV-Vis absorption spectra were (DRS) were collected using a Shimadzu UV-Vis 2550 spectrophotometer. Reflectance measurements were performed on powdered samples, using a standard $BaSO_4$ as a reference.

1.4 Photocatalytic analysis

The photocatalytic activity of as-prepared samples was evaluated by the degradation of MB. A 250 W xenon lamp with a cut-off filter was used to remove the wavelength less than 420 nm. In details, 50 mg of the sample powers were dispersed into the 100 mL solution of MB (10 mg·L^{-1}), in order to insured the adsorption equilibrium, the suspensions were kept stirring for 30 min in darkness before irradiation. At the same irradiation intervals, 6 mL aqueous solution were sampled and separated from the suspended catalyst particles for analysis. The photocatalytic degradation ratio was tested via the intensity changes of the absorption peak at 664 nm to determine the concentration of MB at different times by the same UV-Vis spectrophotometer (UV-2550, Shimadzu, Japan).

2 Results and discussion

2.1 Morphology and structure

The morphology of as-prepared samples was detected by SEM. The $MnNb_2O_6$ exhibited a uniform hexagonal nanoflower structure with excellent dispersion in Fig.1a. From the SEM image of RGO-$MnNb_2O_6$ in Fig.1b, the RGO layer could be observed in certain positions because of the tight contact between $MnNb_2O_6$ and RGO. Fig.1c showed the TEM of single hexagonal nanoflower $MnNb_2O_6$. The TEM of single RGO was shown in Fig.1d, the obvious wrinkles and folds exhibited clearly the 2D structure of the transparent graphene sheets. In RGO-$MnNb_2O_6$ composites (Fig.1e), RGO sheets were uniformly attached on $MnNb_2O_6$ surfaces. The HRTEM image of composites in Fig.1f was further to characterize the structure of RGO-$MnNb_2O_6$, the distinct lattice fringes with spacing of 0.167 nm corresponded well to the (311) facet of $MnNb_2O_6$.

The crystalline phases of the composites were investigated via XRD. As shown in Fig.2, the pristine $MnNb_2O_6$ showed a series of sharp diffraction peaks, which can be indexed into columbite phase (JCPDS

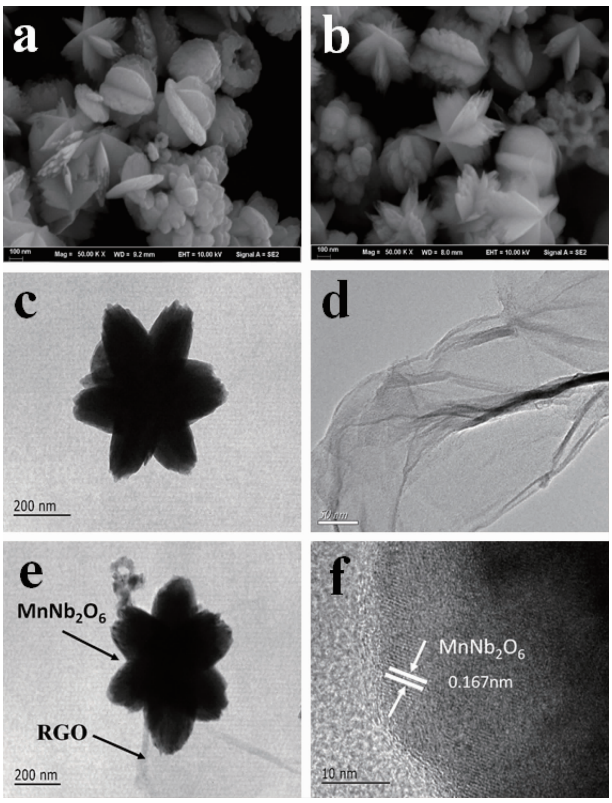

Fig.1 SEM images of $MnNb_2O_6$ (a) and RGO-$MnNb_2O_6$ (b); TEM images $MnNb_2O_6$ (c), GO (d) and 3% RGO-$MnNb_2O_6$ (e); HRTEM image of 3% RGO-$MnNb_2O_6$ (f)

72-0484) with no observable impurities. For the RGO-$MnNb_2O_6$ composites, with increasing the amount of RGO, no obvious changes were found in these patterns, which suggested that the introduction of RGO had no obvious influence on the $MnNb_2O_6$ crystalline structure. Notably, no diffraction peaks of RGO could be observed in the RGO-$MnNb_2O_6$ composites, which may be due to the low amount of RGO. On the other hand, the main characteristic peak of RGO at 24.5° may be overlapped with the strong peak of $MnNb_2O_6$ at 24.1°.

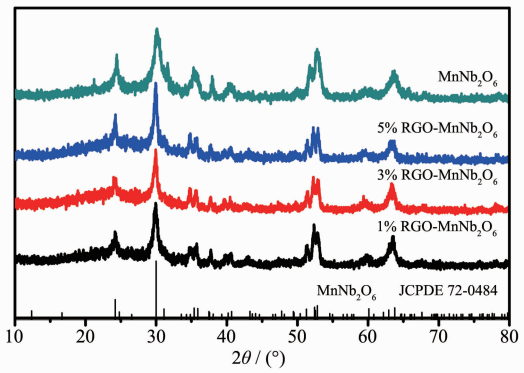

Fig.2 XRD patterns of as-prepared samples

2.2 UV-Vis absorption spectra

The light absorption spectra of $MnNb_2O_6$ and 3% RGO-$MnNb_2O_6$ samples were investigated by the UV-Vis absorption. As shown in Fig.3, bare $MnNb_2O_6$ showed strong absorption in the visible light range with the obvious absorption edge around 560 nm, it could be found that $MnNb_2O_6$ was a narrow band gap semiconductor with the band gap was about 2.2 eV. When the 3% RGO were decorated with the $MnNb_2O_6$, the light absorption spectrum had a strong absorption over 560 nm, which illustrated that the RGO can strengthen the visible-light spectral responsive range. Similar phenomena were also observed by other researchers, which can be ascribed to the absorption of RGO[31].

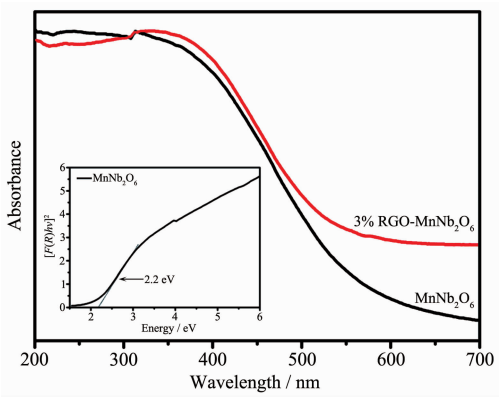

Fig.3 UV-Vis adsorption spectra with as-prepared samples and calculated band gap

The Raman absorption spectra of pure $MnNb_2O_6$, GO and RGO-$MnNb_2O_6$ were exhibited in Fig.4. The recorded spectrum of GO exhibited two characteristic peaks located at 1 352 and 1 585 cm^{-1}, corresponding to the D and G band, respectively[27]. In general, it was accepted that the ratio of the D to G band intensity (I_D / I_G) was related to the density of defects in graphene-based materials and the graphitization degree of carbonaceous materials. The peak intensity I_D / I_G were 0.99 of GO to 1.12 of RGO-$MnNb_2O_6$, the enhanced peak intensity ratios could be contributed to more defects introduced into the RGO-$MnNb_2O_6$, demonstrating the GO was reduced to RGO.

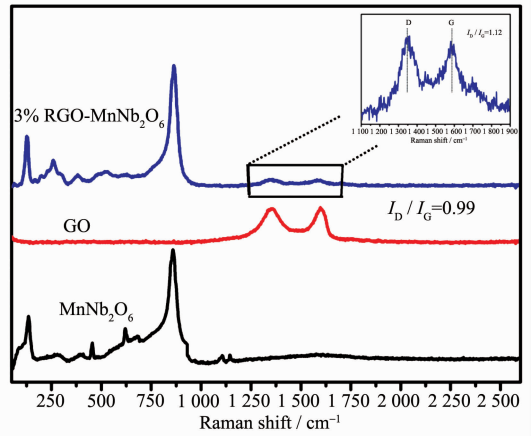

Fig.4 Raman spectra of $MnNb_2O_6$, GO and 3% RGO-$MnNb_2O_6$

2.3 XPS analysis

XPS was carried out to analyze the surface chemical compositions of 3% RGO-$MnNb_2O_6$ photocatalysts in Fig.5. According to the entire XPS spectrum observations in Fig.5a, the peaks of Bi, Nb, O and C were all existed in the 3% RGO-$MnNb_2O_6$ sample. Fig.5b displayed two strong peaks at 641.1 and 653.6 eV, which assigned to Mn2*p*. The two peaks for Nb3*d* centered at 207.3 and 210.1 eV in Fig.5c. Additionally, the XPS signal of O1*s* was locating at 530.5 eV in Fig.5d. The C1*s* spectrum (Fig.5e) of the 3% RGO-

$MnNb_2O_6$ sample could be fitted into three peaks located at 284.8, 285.9 and 287.7 eV, which corresponded to C-C, C-O, and C=O, respectively. The peak intensity of C-C was much higher than that of the C-O and C=O, which suggested that most of the oxygen-containing groups were removed and the GO was reduced to RGO.

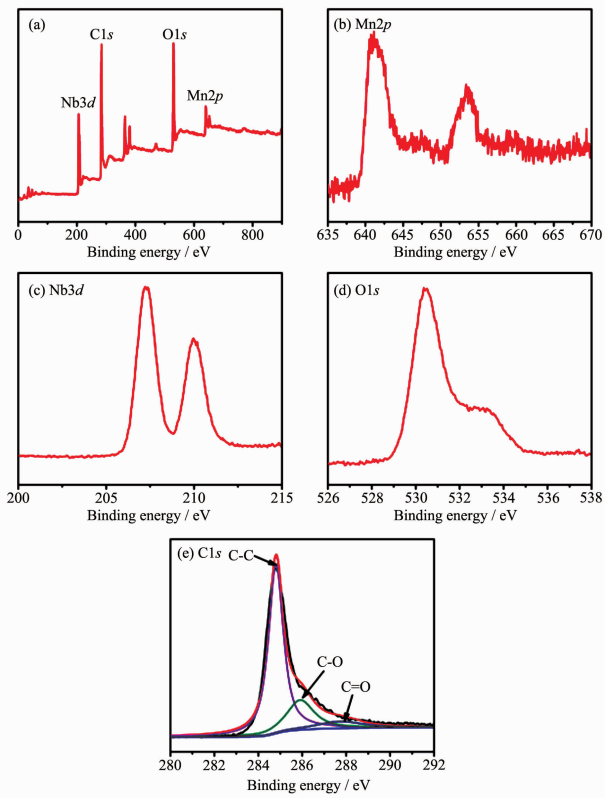

(a) survey spectrum, (b) Mn2*p*, (c) Nb3*d*, (d) O1*s* and (e) C1*s*

Fig.5　XPS spectra of 3% RGO-$MnNb_2O_6$ samples

2.4　Photocatalytic behaviors

In this work, MB was chosen as the target pollution to assessed the photocatalytic performance in Fig.6a. Under 60 min irradiation, 38.5% of MB was degraded by pure $MnNb_2O_6$. With respected to the composites of RGO-$MnNb_2O_6$, when the two semiconductors were coupled together, the photocatalytic activities could be significantly enhanced in comparison to the pure $MnNb_2O_6$ catalysts, the MB degradation ratio of the 3% RGO-$MnNb_2O_6$ sample arrived 78.2%. However, when the RGO amount was further increased from 3% to 5%, the MB degradation ratio would be decreased, which should be because of large RGO amount (over 3%) may result from the limited light absorption.

The degradation kinetics of MB by using as-prepared samples were investigated and the results were shown in Fig.6b. It can be observed that the changes of the MB concentration vs the irradiation time over the as-prepared samples conformed to the pseudo-first-order kinetics plot. The reaction rate constant (k) values enhanced through the introduction of RGO. The 3% RGO-$MnNb_2O_6$ sample (0.025 4 min^{-1}) exhibited the highest k value among all the samples, which was about 3.26-fold higher than that of pure $MnNb_2O_6$ (0.007 84 min^{-1}).

2.5　Optical and electronic properties

Photoluminescence (PL) was employed to study the recombination abilities of photoexcited electron-hole pairs. A lower PL intensity revealed the lower photoinduced charge carriers′ recombination. Fig.7 exhibited the PL emission spectra of pure $MnNb_2O_6$ and 3% RGO-$MnNb_2O_6$ samples, in which both the samples showed a strong emission peak centered at around 470 nm with an excitation wavelength of 360 nm. Remarkably, the 3% RGO-$MnNb_2O_6$ displayed a

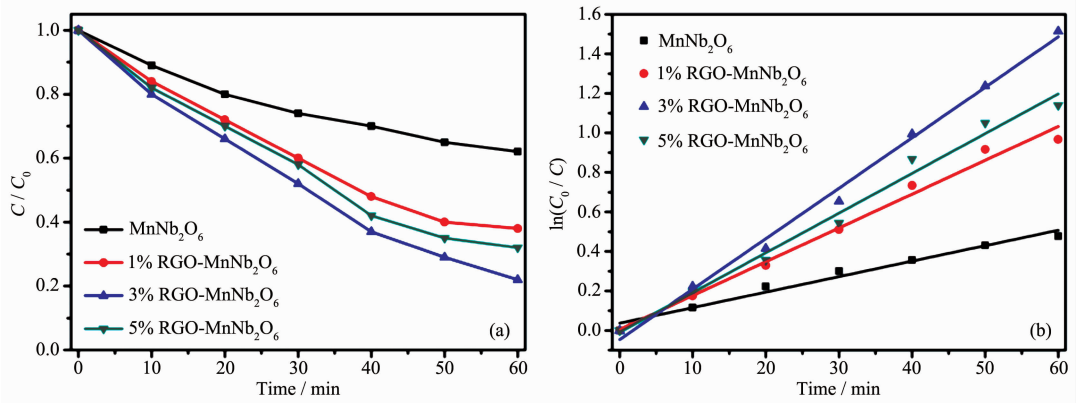

Fig.6　Photocatalytic degradation of MB with as-prepared samples (a); Pseudo-first-order reaction kinetics for MB degradation (b)

lower PL intensity than the sample of $MnNb_2O_6$, which indicated that the recombination of photogenerated charge carriers was inhibited in the 3% RGO-$MnNb_2O_6$ composite.

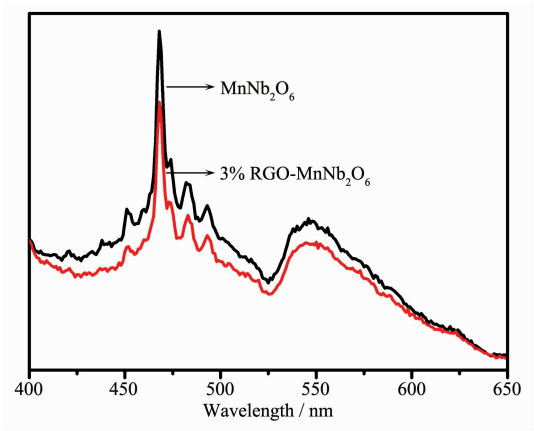

Fig.7 PL spectra and fluorescence decay curves of the $MnNb_2O_6$ and 3% RGO-$MnNb_2O_6$ sample

2.6 Photocatalytic mechanism

A series of active species trapping experiments were carried out to examine the photocatalytic oxidation mechanism with RGO-$MnNb_2O_6$ sample. In Fig.8, when 1 mmol·L^{-1} triethanolamine (TEA)[32-36] was added to trap the holes (h^+), the photodegradation ratio was signicantly declined in comparison to the reaction without TEA, revealing that the photogenerated holes (h^+) played major role in the selective oxidation of pollutant. As 1 mmol·L^{-1} BQ[31] was added to trap ·O_2^-, the photodegradation ratio decreased to 50.4% , therefore, it can be concluded that ·O_2^- took part in the oxidation reaction. On the contrary, the addition of 1 mmol·L^{-1} IPA (71.8%) to trapped the ·OH, the photocatalyst degradation ratio had little influence.

To illustrate the photocatalytic process for decomposing organic dyes by RGO-$MnNb_2O_6$ composite, we carried out band position calculations by a plain method according to the previous paper. We can evaluate the conduction band of semiconductor by the formula[37]:

$$E_{CB}=X-E_e-0.5E_g$$

where E_{CB} was the CB edge potential; X was the electronegativity of the semiconductor, which was the geometric mean of the electronegativity of the constituent atoms ($MnNb_2O_6$ was 6.05); E_e was the energy of free electrons on the hydrogen scale (4.5 eV); and E_g was the band gap energy of the semiconductor. The E_{VB} value can be obtained by $E_{VB}=E_{CB}+E_g$. As the band gap of $MnNb_2O_6$ was 2.2 eV by the UV-Vis diffuse reflectance absorption spectra, the conduction band (CB) of $MnNb_2O_6$ was calculated to be 0.45 eV, and the valence band (VB) of $MnNb_2O_6$ was calculated to be 2.65 eV. On the basis of active species trapping experiments and calculated energy bands, a possible photocatalytic mechanism of RGO-$MnNb_2O_6$ can be drawn as shown in Fig.9. When the RGO-$MnNb_2O_6$ sample subjected to the irradiation of visible light, the electrons could be excited form the VB to the CB with simultaneous generation of holes in the VB. MB molecules adsorbed on the surface of $MnNb_2O_6$ were directly oxidized by h^+, besides, h^+ also have few opportunities to react with OH^-/H_2O to form ·OH radicals. The photo-generated e^- in the CB can be injected into RGO, therefore hindering the recombination process of the e^--h^+ pairs and leading to an effective charge separation and stabilization. On the

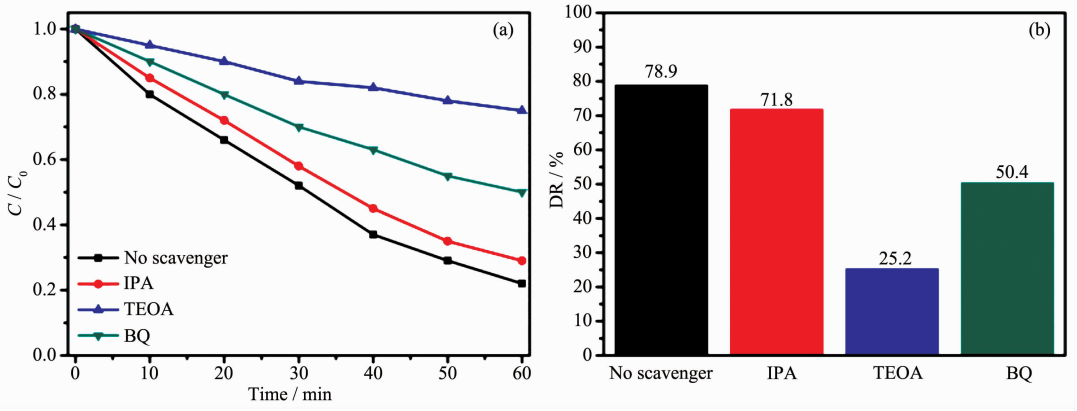

Fig.8 Photocatalytic degradation ratios of MB using different radical scavengers over 3% RGO-$MnNb_2O_6$ sample

other hand, e^- could transport along the RGO sheets from inner region to the surface and react with O_2 to form $\cdot O_2^-$ radicals, although $\cdot O_2^-$ radical was not efficient in the degradation of aromatic compounds such as MB molecules.

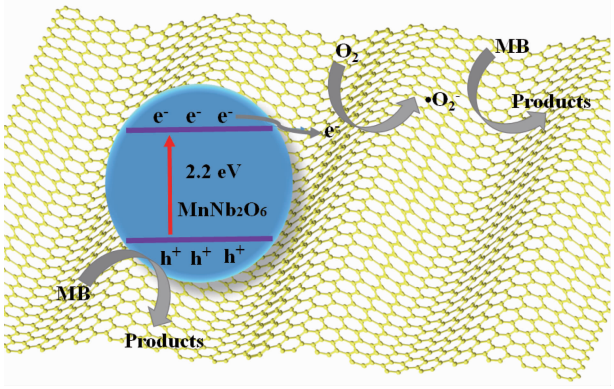

Fig.9　Schematic of the separation and transfer of photogenerated charges in the RGO-$MnNb_2O_6$ sample combined with the possible reaction mechanism of photocatalytic procedure

3　Conclusions

In summary, we have successfully constructed the RGO-$MnNb_2O_6$ composites with the hydrothermal and photo-reduction processes. The 3% RGO-$MnNb_2O_6$ sample exhibited best photocatalytic performance for the degradation of MB, which was about 2 times higher than that of bare $MnNb_2O_6$. The enhanced photocatalytic activity toward photodegrading MB under visible light irradiation could be ascribed to high charge carrier mobility of RGO, which greatly promoted efficient separation of the photoexcited electron-hole pairs as well as depressed recombination of the charge carriers. The as-designed principles outlined in this paper can be extended to other semiconductors to enhance the nanoscale heterostructures undergoing development for solar energy conversion.

Acknowledgements: The authors would like to acknowledge the National Natural Science Foundation of China (Grants No.21303074), Natural Science Foundation of Jiangsu Province (Grant No.BK20141304), Special Financial Grant from the China Postdoctoral (Grant No.2015T80500), China Postdoctoral Science Foundation funded project (Grant No. 2014M551508).

References:

[1] Hernando M D, Vettori S D, Martinez Bueno M J, et al. *Chemosphere*, **2007**,**68**:724-730
[2] Jain R, Mathur M, Sikarwar S, et al. *J. Environ. Manage.*, **2007**,**85**:956-964
[3] Hamdaoui O. *Desalination*, **2011**,**271**:279-286
[4] Zhang W L, Li Y, Wang C, et al. *Desalination*, **2011**,**266**:40-45
[5] Hoffmann M R, Martin S T, Choi W, et al. *Chem. Rev.*, **1995**, **95**:69-96
[6] Lee H, Choi J, Lee S, et al. *Appl. Catal. B*, **2013**,**138**:311-317
[7] Singh S A, Madras G. *Sep. Purif. Technol*, **2013**,**105**:79-89
[8] Katsumata H, Oda Y, Kaneco S, et al. *RSC Adv.*, **2013**,**3**: 5028-5035
[9] Pei C C, Leung W W. *Sep. Purif. Technol*, **2013**,**114**:108-116
[10]Jiang Y, Amal R. *Appl. Catal. B*, **2013**,**138**:260-267
[11]Wetchakun N, Chaiwichain S, Inceesungvorn B, et al. *ACS Appl. Mater. Interfaces*, **2012**,**4**:3718-3723
[12]Li H P, Liu J G, Hou W G, et al. *Appl. Catal. B*, **2014**,**160**: 89-97
[13]Wang T, Li C J, Ji J Y, et al. *ACS Sustainable Chem. Eng.*, **2014**,**2**:2253-2258
[14]Fujishima A, Zhang X, Tryk D A. *Surf. Sci. Rep.*, **2008**,**63**: 515-582
[15]Chen X B, Shen S H, Guo L J, et al. *Chem. Rev.*, **2010**,**110**: 6503-6570
[16]Gao F, Chen X Y, Yin K B, et al. *Adv. Mater.*, **2007**,**19**: 2889-2892
[17]Zhang L S, Wang W Z, Chen Z G, et al. *J. Mater. Chem.*, **2007**,**17**:2526-2532
[18]Cha H G, Kim S J, Lee K J, et al. *J. Phys. Chem. C*, **2011**, **115**:19129-19135
[19]Bi Y P, Ouyang S X, Umezawa N, et al. *J. Am. Chem. Soc.*, **2011**,**133**:6490-6492
[20]Xu J, Li Y, Peng S, et al. *Phys. Chem. Chem. Phys.*, **2013**, **15**:7657-7665
[21]Li Y, Wang J, Peng S, et al. *Int. J. Hydrogen Eenergy*, **2010**, **35**:7116-7126
[22]Xu J, Li Y, Peng S. *Int. J. Hydrogen Energy*, **2015**,**40**:353-362
[23]Hu B, Cai F P, Shen H, et al. *CrystEngComm*, **2014**,**16**: 9255-9265
[24]Tan L L, Chai S P, Mohamed A R. *ChemSusChem*, **2012**,**5**: 1868-1882
[25]Huang X, Qi X Y, Boey F, et al. *Chem. Soc. Rev.*, **2012**,**41**: 666-686

[26]Zhang W, Li Y, Peng S, et al. *Beilstein J. Nanotechnol.*, **2014**,**5**:801-811

[27]Li Y, Wang H, Peng S. *J. Phys. Chem. C*, **2014**,**118**:19842-19848

[28]Ng Y H, Iwase A, Kudo A, et al. *J. Phys. Chem. Lett.*, **2010**, **1**:2607-2612

[29]Wang C, Zhang G, Zhang C, et al. *J. Colloid Interface Sci.*, **2014**,**435**:156-163

[30]Xu Y, Bai H, Lu G. *J. Am. Chem. Soc.*, **2008**,**130**:5856-5857

[31]Yan Y, Wang C, Yan X, et al. *J. Phys. Chem. C*, **2014**,**118**: 11823519-23526

[32]Gao J, Liu F, Liu Y. *Chem. Mater.*, **2010**,**22**:2213-2218

[33]Li G, Wong K, Zhang X, et al. *Chemosphere*, **2009**,**76**:1185-1191

[34]Liu S, Zhang N, Tang Z. *ACS Appl. Mater. Interfaces*, **2012**, **4**:6378-6385

[35]Yan S C, Li Z S, Zou Z G. *Langmuir*, **2010**,**26**:3894-390

[36]Joshi U A, Darwent J R, Yiu H P. *J. Chem. Technol. Biotechnol.*, **2011**,**86**:1018-1023

[37]Wang S, Li D, Sun C. *Appl. Catal. B*: *Environ.*, **2014**,**144**: 885-892